Separation and Purification Technology 235 (2020) 116284

Contents lists available at ScienceDirect

Separation and Purification Technology

journal homepage: www.elsevier.com/locate/seppur

Kinetic study of vacuum evaporation of elements from ternary melts; case of dilute solution of P in Si-Al melts

Arman Hoseinpur[a,c,*], Kai Tang[b], Jafar Safarian[a,c]

[a] Department of Materials Science and Engineering, Norwegian University of Science and Technology (NTNU), 7034 Trondheim, Norway
[b] SINTEF Industry, 7465 Trondheim, Norway
[c] Norwegian Center for Sustainable Solar Cell Technology (www.susoltech.no), Norway

ARTICLE INFO

Keywords:
Kinetics
Vacuum refining
Evaporation
Silicon (Si)
Phosphorus (P) removal
Aluminum (Al) removal
Hertz-Knudsen-Langmuir

ABSTRACT

This research is devoted to study phosphorus removal from Si-Al alloys by vacuum refining of the ternary system of dilute solutions of P in Si-20 wt%Al. The experiments were carried out in an induction furnace and after the refining process, the melt was characterized by ICP-MS technique to trace the concentration change of the volatile elements. The experimental results show that P removal from Si-Al-P melts takes place faster compared to Si-P melts and Al evaporates during the vacuum refining as well. The empirical kinetics of P and Al evaporation is discussed and the apparent activation energy for P and Al evaporation from Si-Al melts is obtained as E_P = 249.4 kJ·mol^{-1}and E_{Al} = 144.8 kJ·mol^{-1} respectively. Results show that the composition of the melt changes continuously during the refining process due to rapid Al evaporation. In order to investigate the evaporation kinetics of the melt constituents, we developed a numerical approach by applying the Hertz-Knudsen-Langmuir equation for evaporation. This approach can be applied to model the evaporation of the melt constituents in a ternary system whose composition changes during the vacuum refining process. The model is validated with performed experimental results and it can be applied to discuss the effect of temperature, pressure, initial melt composition on the time of vacuum refining.

1. Introduction

Various refining procedures of Silicon (Si) have been investigated widely in recent years due to the application of ultra-high pure silicon for making solar panels [1,2]. Currently, 0.5% of world energy is produced by means of solar energy, and it is forecasted to produce 32% of the world energy in the year 2070 by solar panels [3].The statistics show that over 95% of the solar power is now generated by Si solar panels that are expected to be the main solar power producers in future [4]. Thus, low cost and sustainable production of solar grade silicon would be necessary to pave the way for the solar industry growth in the coming decades. Silicon is produced by the carbothermic reduction of quartz (SiO_2) in submerged arc furnace [5,6]. The product of this process is called metallurgical grade silicon (MG-Si) and can have a purity of around 99% [7]. The MG-Si can be refined by the Siemens® and fluidized bed reactor (FBR) methods to much higher purities up to, i.e, 6N-11N [8]. Metallurgical processes can be applied for refining of Si up to the purity of 6N, accompanying with less CO_2 emissions and less energy consumption [9]. Up to now vacuum refining [10–13], gas refining [14,15], slag refining [16,17], solvent refining [18–21], leaching [22,23], and directional solidification [18] procedures have been studied for refining of Si. These processes are scalable and are applied by the industries to produce SoG-Si such as Elkem® (slag refining and leaching[24]), Silicor® (Solvent refining and leaching [25]), and Ferroglobe® (slag and vacuum [26]). It is worth to note that phosphorus (P) is one of the most challenging impurities in Si to control since it has detrimental effects on the efficiency of solar panels. In addition, P is a tough element to be removed from Si since it has a large segregation coefficient (0.35) and cannot be removed efficiently by directional solidification method.

Vacuum refining is an efficient technique for the removal of volatile species from the melts and it has been applied for the refining of various alloys like steels [27–29], Ni superalloys [30], aluminum alloys [31], copper [32,33], platinum [34], and Si [11,12,35–39].The driving force for vacuum refining is the difference between the vapor pressure of the volatile impurity and that for the molten metal [40–42]. Thus, vacuum refining would be an effective refining method for removing P from Si due to the considerable difference of the P vapor pressure with the Si vapor pressure [43]. Vacuum refining of Si has been researched since 1994 [44] and well discussions the mechanism of P evaporation from Si

* Corresponding author at: Department of Materials Science and Engineering, Norwegian University of Science and Technology (NTNU), 7034 Trondheim, Norway.
E-mail address: arman.h.kermani@ntnu.no (A. Hoseinpur).

https://doi.org/10.1016/j.seppur.2019.116284
Received 29 June 2019; Received in revised form 12 October 2019; Accepted 2 November 2019
Available online 11 November 2019

is presented in previous study [43,45–48]. The effect of temperature and chamber pressure on the kinetics of P evaporation has been studied [12,13] and it has been shown that higher temperatures and lower chamber pressures can speed up he P evaporation from Si. Although the effect of other impurities in MG-Si on P removal kinetics have been studied in a few works [49,50] the vacuum refining of Si alloys with considerable amount of a secondary element, i.e. Al in this study, has not been investigated yet.

This research is devoted to the investigation of the effect of Al addition on vacuum refining of P from Si by performing the vacuum refining on a Si-20Al alloy. It worth to note that Al has higher vapor pressure than Si and it can also be removed by vacuum refining [40,51]. In addition, Since the melting point of Al (660 °C) is lower than the melting point of Si (1414 °C), all the melts in the binary system of Si-Al possess lower liquidus point than the melting point of Si. This would make it possible to carry out the vacuum refining process at temperatures even lower than the melting point of Si which can lead to considerable decrease in Si loss.

2. Experimental procedure

In this research we used of A commercial grade silicon (HQ-Silgrain®) with the purity of 99.76% and Al (99.99 wt%) was used as the initial materials to make Si-20 wt% Al alloy. The experiments were carried out in an induction furnace able to work in both vacuum and Ar gas atmosphere conditions. A schematic representation of the furnace can be found in previous study [43]. In order to make the Si-Al alloy, 172 g of Silgrain® with 43 g of Al (totally 215 g of Si and Al, and the A/V = 30 m^{-1}) was charged into a SiC crucible. The authors have studied the interaction of Si-20 wt% Al with graphite and SiC crucibles in [52], where it is shown that up to about 70 wt% Al the SiC crucible shows no interaction with Al in the melt while graphite crucible degrades with Al. Thus, the experiments of this research are done in SiC crucibles. In this research The SiC crucible is put into a bigger graphite crucible. During the experiment the temperature was measured by a thermocouple type "C" (T.C.), which was put in an alumina tube, and was located in between the graphite crucible and the SiC crucible. The whole setup was wrapped with graphite wool and mica sheet for safety reasons and put in the copper coil. A schematic of the setup configuration can be found in [43]. Before starting the experiment, the chamber was vacuumed completely and subsequently it was filled by Ar (99.9999%) up to 1000 mbar and vacuumed again. This process was repeated for three times to make sure Ar has purged the chamber and there is no air left in. Subsequently the heating process was started while Ar was flushing to the chamber keeping the pressure around 1040–1050 mbar. The temperature–time profile of the experiment done on the 1500 °C is plotted in the Fig. 1. As we started the heating process temperature rose up and by reaching to the melting point Al, it melted, as shown in Fig. 1b. Subsequently the Si dissolved into the melted Al at higher temperatures. When all the Si was dissolved into the melt and a homogenous melt was formed in the crucible, a sample was taken from the melt by a specific sampling device to characterize the initial concentration of the alloy. Subsequently, the alloy temperature was adjusted on the target temperature (1400 °C and 1500 °C) and then the chamber was vacuumed. It was observed that the pressure of the chamber decreased to around 1–3 and 4–8 Pa in the experiments done at 1400 and 1500 °C, respectively. During the refining process, three samples were taken from the melt with 30 min steps. Each time that we needed to take sample, we had to increase the pressure in the chamber by filling it with Ar, to make it easy to take sample from the melt. This made the crucible cool down and the temperature to decrease. All the sample taken from the alloy were digested in a solution of hydrogen fluoride (HF) and nitric acids (HNO_3). After digestion, the liquor was diluted with distilled water and characterized by the Induction coupled plasma mass spectroscopy (ICP-MS, Agilent − 8800 ICP-MS Triple Quad).

3. Experimental results and discussion

The experimental results and observations of the refining process are presented in Section 3.1. Further discussions about the empirical kinetics of P and Al removal form Si-Al melts is presented the Section 3.2.

3.1. Experimental results

Table 1 presents the concentrations of P and Al in the Si-Al melt after various steps of vacuum refining. This table shows that after 90 min of the refining process, about 35% and 65% of P is removed from the Si-Al alloy at 1400 °C and 1500 °C, respectively. Compared with literature works on vacuum refining of Si [10,13,43], this result shows that by alloying Si with Al, it is feasible to effectively remove P from the Si-Al alloy at temperatures even lower than the melting point of Si. In addition, Table 1 shows that Al concentration in the melt decreases by time of the refining process. This table shows after 90 min of vacuum refining 34% and 42.9% of Al evaporates at 1400 °C and 1500 °C, respectively.

3.2. Mass transfer coefficient for P and Al removal

Vacuum evaporation of P from the Si melt has been investigated in [10,13,43,44], where it is shown that P mainly evaporates from the melt as the monoatomic gas, $P_{(g)}$. the thermodynamics of Si-P melts are also studied in [53–55] where it is shown that $P_{(g)}$, $P_{2(g)}$, $P_{4(g)}$ gases exist in the binary system of Si-P, but at dilute solutions of P (ppm levels) only monoatomic form of the P becomes stable. Miki [53] has shown at 1550 °C up to about 50 ppmM of P in Si, the monoatomic form of P is the major gas in equilibrium with Si and if the P concentration exceeds this limit, $P_{2(g)}$ becomes the major gaseous species in equilibrium with Si melt. In addition to phosphorus, the Al evaporation from Si in vacuum conditions has also investigated in [13], where it is indicated that the first order kinetic model can be applied on the Al evaporation from Si melt. Therefore, with regard to the previous studies, in order to obtain the rate constant for the P and Al removal from Si-20Al alloy, here we consider the first order kinetic model [56], which can be expressed as follows:

$$\ln\left(\frac{C_{i,0}}{C_{i,t}}\right) = k_i \cdot \left(\frac{A}{V} \cdot t\right) \quad (1)$$

where $C_{i,0}$ and $C_{i,t}$ show the initial and instant concentrations of element i in melt, A and V are the melt surface area and volume, respectively. The k_i is called the rate constant of evaporation for element i. By inserting the experimental data presented in Table 1 into Eq. (1) and by plotting the left side of this equation as a function of $\left(\frac{A}{V}. t\right)$, the k_i can be obtained as the slope of the plotted curves. Fig. 2a shows the effect of temperature on the kinetics of P removal from the Si-20wt.%Al alloy, and it shows that the first order reaction model fits to the experimental data. It is worth to be mentioned that we tried the kinetic model for 2nd order reactions as well, however, it showed a weak correspondence to the experimental data, and thus same as the Si melt, P and Al removal from Si-20Al alloy is of 1st the order and hence we can consider the evaporation of P and Al from the melt taking place through the following reaction,

$$P = P_{(g)} \quad (2)$$

$$Al = Al_{(g)} \quad (3)$$

Fig. 2a shows that by increasing the temperature from 1400 °C to 1500 °C the slope of the lines fitted to the experimental data becomes steeper and the empirical rate constant k_P increases significantly from 2.18 to 5.7 μm s^{-1}. In order to investigate the dependence of k_i to temperature we can apply the Arrhenius equation presented as follows,

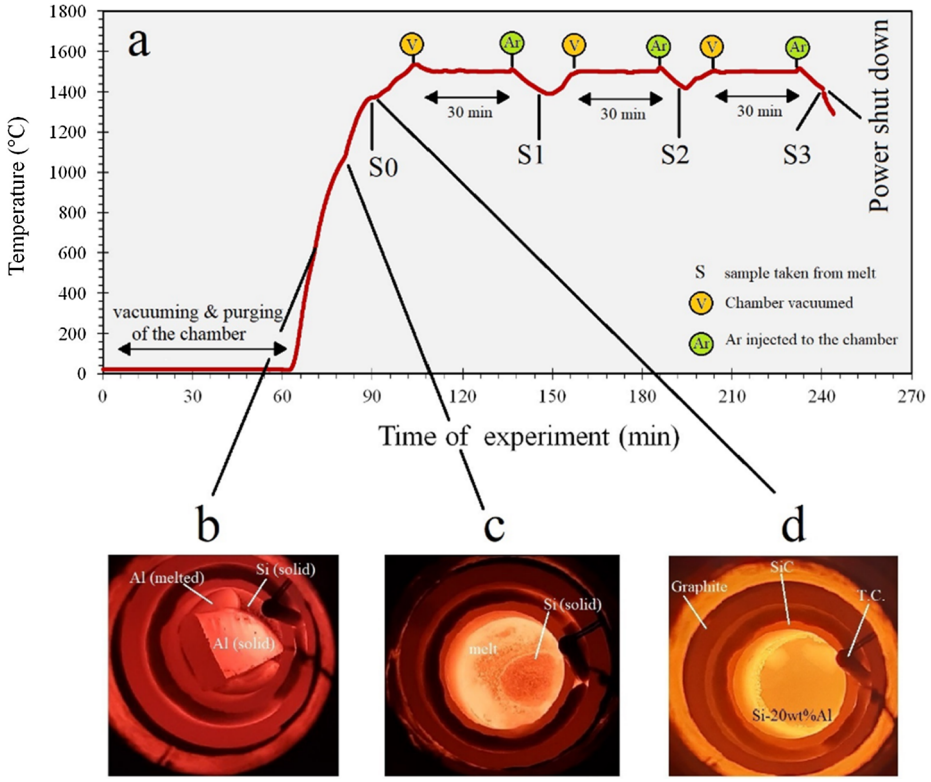

Fig. 1. (a): Temperature profile and the experiment details of the experiment done at 1500 °C and the photos of the melt surface at the; Al melting (b), Si dissolving into the melt (c), and after the total melting of the whole materials in the crucible (d).

Table 1
The measured concentrations of P and Al in the melt after various times of vacuum refining (10^{-4}wt. % = ppmM).

Temperature (°C)	Al (wt.%)				P (wt.%)			
	Initial composition	30 min	60 min	90 min	Initial composition	30 min	60 min	90 min
1400	19.95	18	16.24	13.35	18×10^{-4}	15.53×10^{-4}	14×10^{-4}	12.87×10^{-4}
1500	20	18	12.27	11.39	18×10^{-4}	12.75×10^{-4}	11.13×10^{-4}	6.5×10^{-4}

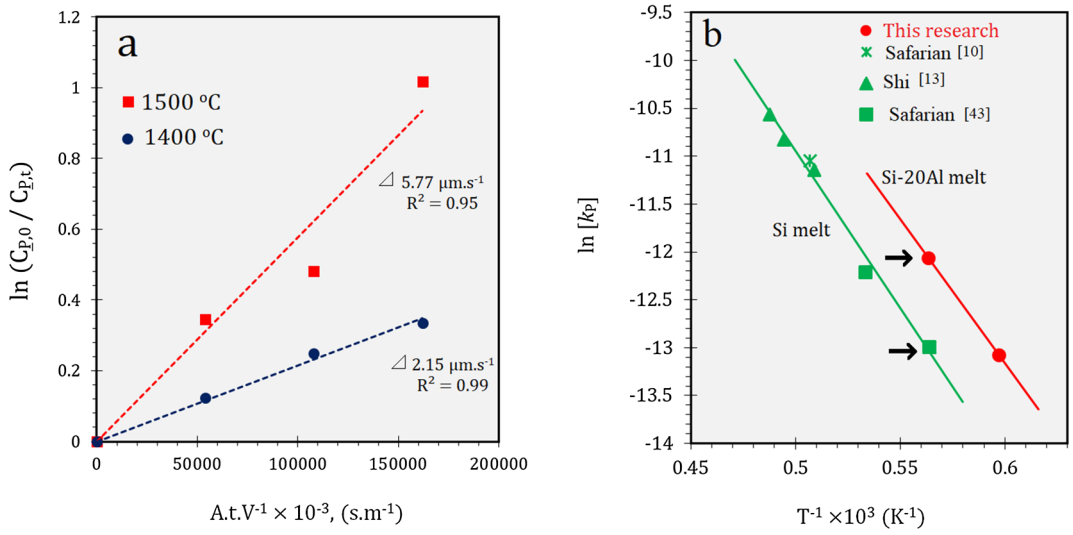

Fig. 2. (a): Relationship between $\ln\frac{C_{P,0}}{\bar{C}_{P,t}}$ and $\left(\frac{A}{V}\cdot t\right)$ for phosphorus removal from Si-20Al at various temperatures (b): A comparison of P removal from Si and Si-20Al alloy as a function of reciprocal absolute temperature.

Table 2
Comparison of the kinetic parameters calculated for P removal from Si, P and Al removal from Si-Al by vacuum refining.

Element (i)	Melt composition, Research	E_i (kJ mol^{-1})	ln (k^*_i μm s^{-1})
P	Si [43], Si [10], Si [13]	273	5.48
P	Si-20Al (this research)	249.4	4.87
Al	Si-20Al (this research)	144.8	−2.6

$$\ln(k_i\left[\frac{\mu m}{s}\right]) = \ln k_i^* - \frac{E_i}{\mathrm{R}.\ T} \tag{4}$$

where k_i^* is a constant called frequency factor, E_i is the apparent activation energy for the evaporation of the element i, and T denotes the absolute temperature. By plotting the rate constants of P evaporation obtained at various temperatures versus the reversed absolute temperature (T^{-1}), the E_i and k_i^* can be obtained. The obtained relationship between $\ln(k_P)$ and T^{-1} for P evaporation from Si-Al melt is presented in Fig. 2b. In addition to our experimental data, we applied the data published in the literature [10,13,43] to obtain the relation between $\ln k_P$ and T^{-1} for P evaporation from Si. Fig. 2b shows that the line belonging to P evaporation from Si-Al alloy is located above the line of P evaporation from Si over a wide range of temperature. This indicates that P evaporation from Si-Al alloy is faster than Si melt. In order to provide a better view about the effect of Al, we should compare the magnitude of the two experimental points that are marked by the arrows in Fig. 2b. Although both experiments are done at the same temperature, k_P is 2.6 μm s^{-1} in the case of Si melt [43], while it is 5.7 μm s^{-1} (2.2 times greater) in the case of Si-Al alloy. Table 2 shows the experimental conditions and the calculated E_P for P removal from Si and Si-Al melt. As can be seen in Table 3, the E_P for P evaporation is 23.6 kJ mol^{-1} lower in the case of Si-Al melt. This reveals Al contributes to accelerating the P evaporation by decreasing the E_P for P evaporation. The k_P^* for P evaporation from Si and Si-Al melt is also presented in the Table 2, and can be seen that the k_P^* has decreased from 240.45 to 130.45 for Si and Si-Al melts, respectively. It should be mentioned that the decrease in k_P^*leads the kinetic line for P removal in Fig. 2b to shift down. By considering the kinetic model of 1st order reaction presented in equation (1), it can be concluded that for making the rate constant 2.2 times greater the apparent energy needs to decrease only12.62 kJ. However, Table 2 shows that Al addition to the Si has led the E_P to decrease by 23.6 kJ mol^{-1}, which is more than the theoretical calculations. This shows the positive effect of decreasing E_P with Al addition is canceled partially out by the decrease in k_P^*).

The empirical kinetics of Al evaporation from the Si-Al melt is investigated here by using the same method we applied to study the kinetics of P evaporation. Fig. 3a represents the effect of temperature on the kinetics of Al evaporation from Si at 1400 and 1500 °C temperatures. Fig. 3a shows that Al evaporation from Si takes place through a 1st order reaction and the rate of Al evaporation increases from 2.28 to 3.8 μm s^{-1} as the temperature of process is increased from 1400 °C to 1500 °C. With applying experimental data from literature [13], the dependence of k_{Al} to temperature can also be plotted in Fig. 3b. This figure shows the results of this research correlate well with the results produced by Shi et al. [13]. It is worth mentioning that the initial content of Al in the research of Shi [13] was around 40 ppmM, while the initial content of Al is 20 wt% in this research. This may show that Al evaporation from Si is independent of Al content of the melt and it occurs through a first order reaction in the both dilute and rich Al-containing silicon melts. As presented in Table 2 the E_{Al} = 144 kJ mol^{-1}. A comparison between $E_{Al}$and E_P shows the apparent activation energy for Al evaporation is less than that of P. However, Table 2 shows the refactor parameter for Al evaporation (k_{Al}^*) is considerably smaller than that of P (k_P^*) making the P evaporation faster at higher temperatures and Al evaporation faster at lower pressures. This makes the Al and P to evaporate faster at lower and higher temperatures respectively.

To get a better insight into the Al and P evaporation from Si, we developed the time–temperature (TT) diagrams for evaporation of Al and P from Si and Si-20Al melts presented in Fig. 4. In order to plot the TT diagrams, we should insert the rate constant relations presented in Table 2 into the following equation:

$$x_i^{'}\ [\%] = [1 - \exp(k_i \frac{A}{V} t)] \times 100 \tag{5}$$

where $x_i^{'}$ denotes the mass fraction of element i evaporated from the melt. By rearranging the Eq. (5) we can obtain the time for removing $x_i^{'}$ from melt as follows:

$$t_{x_i^{'}} = \frac{\ln(1 - x_i^{'})}{k_{i,T} \cdot \frac{A}{V}} \tag{6}$$

where $k_{i,T}$ is the rate constant for evaporation of i from melt at temperature T. Fig. 4 is developed for the removal of 1%, 50%, and 99% P and Al from the melt at various temperatures. A comparison between the P evaporation from Si and Si-20Al alloy in Fig. 4a and b shows that P evaporation takes place faster in the Si-20 wt%Al alloy in all temperatures. The TT diagram for Al evaporation is also presented in Fig. 4c. In order to compare the evaporation of P from Si and Si-20 wt %Al, the 99% removal curves of P are compared in Fig. 4d. This figure shows that the P removal curve has shifted to left in the case of Si-20 wt %Al alloy which indicates on faster kinetics of P removal in Si-20Al. The curve belonging to 99% removal of Al is also plotted in Fig. 4d as well. This figure shows the case of Si-20Al alloy, Al removal takes place minimally faster than P removal at temperatures lower than the melting of Si, but at higher temperatures P removal takes place faster. Considering Fig. 4d, three regions can be separated and discussed as follows:

i. low temperatures: where Al removal is faster than P removal from both Si and Si-20Al alloy.
ii. medium temperatures: where P removal from Si-Al melt takes place faster than Al removal.
iii. high temperatures: where P removal from Si takes place faster than Al removal from Si-Al melt.

Regarding these three regions discussed on Fig. 4d, it can be concluded that if vacuum refining at low temperature is demanding, not only the Al addition to the Si accelerates the P removal, but also it makes the vacuum refining to be possible at temperatures lower than the melting point of Si. However, if vacuum refining at shorter time is demanding, it is recommended to perform the process at the second region, where the time for Al removal from Si-20 wt%Al is shorter than the time for P removal from Si melt.

Table 3
Corresponding equations of the flowchart of the applied numerical method presented in Fig. 9.

Step orders' in Fig. 8	Corresponding equation
b	$x_{i,t}^m = \frac{n_{i,t}^m}{n_{i,t}^m + n_{j,t}^m + n_{l,t}^m}$
c	$\gamma_i = f(x_{i,t}^m)$, (See Table A1)
d	$N_{i,t} = \frac{p_{i,t}^e - p_{i,t}^{bp}}{\sqrt{2\cdot\pi\cdot M_i\cdot \mathrm{R}}}$
e	$n_{i,t}^v = A\cdot N_{i,t}^v$(in one second)
f	$x_{i,t}^v = \frac{n_{i,t}^v}{n_{i,t}^v + n_{j,t}^v + n_{l,t}^v}$
g	$p_{i,t}^{bp} = p_t \cdot \sum_{t=0}^{t-1} x_{i,t}^v (p_{i,1}^{bp} = 0)$
h	$n_{i,t}^m = n_{i,t-1}^v (n_{i,1}^v = 0)$

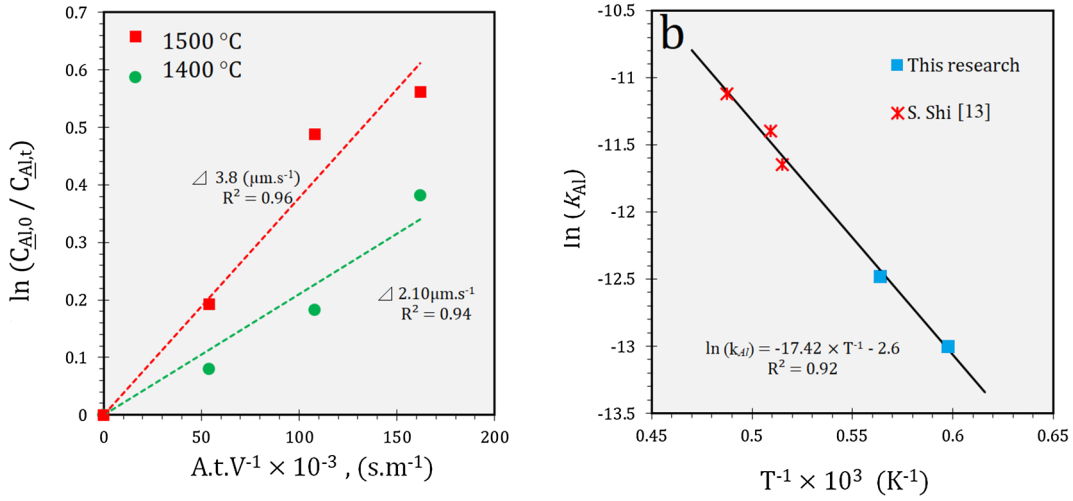

Fig. 3. (a): Relationship between $\ln\frac{C_{Al,0}}{C_{Al,t}}$ and $\left(\frac{A}{V}\cdot t\right)$ for Al removal from melt at different temperatures (b): Relationship of rate constant of Al removal from Si as a function of reciprocal absolute temperature.

4. Hertz-Knudsen-Langmuir evaporation theory; A thermodynamic model for evaporation

In this section we discuss the evaporation of Al and P from Si by applying the Hertz-Knudsen-Langmuir (*HKL*) theoretical model of evaporation. Hertz [57] investigated the evaporation of elements in vacuum condition and later, Knudsen and Langmuir [57] contributed to this topic leading to the generation of HKL equation as follows:

$$N_i\left[\frac{\text{mol}}{m^2.\ s}\right] = \frac{dn_i}{A.\ dt} = \frac{p_i^e - p_i^{bp}}{\sqrt{2\pi M_i RT}} \tag{7}$$

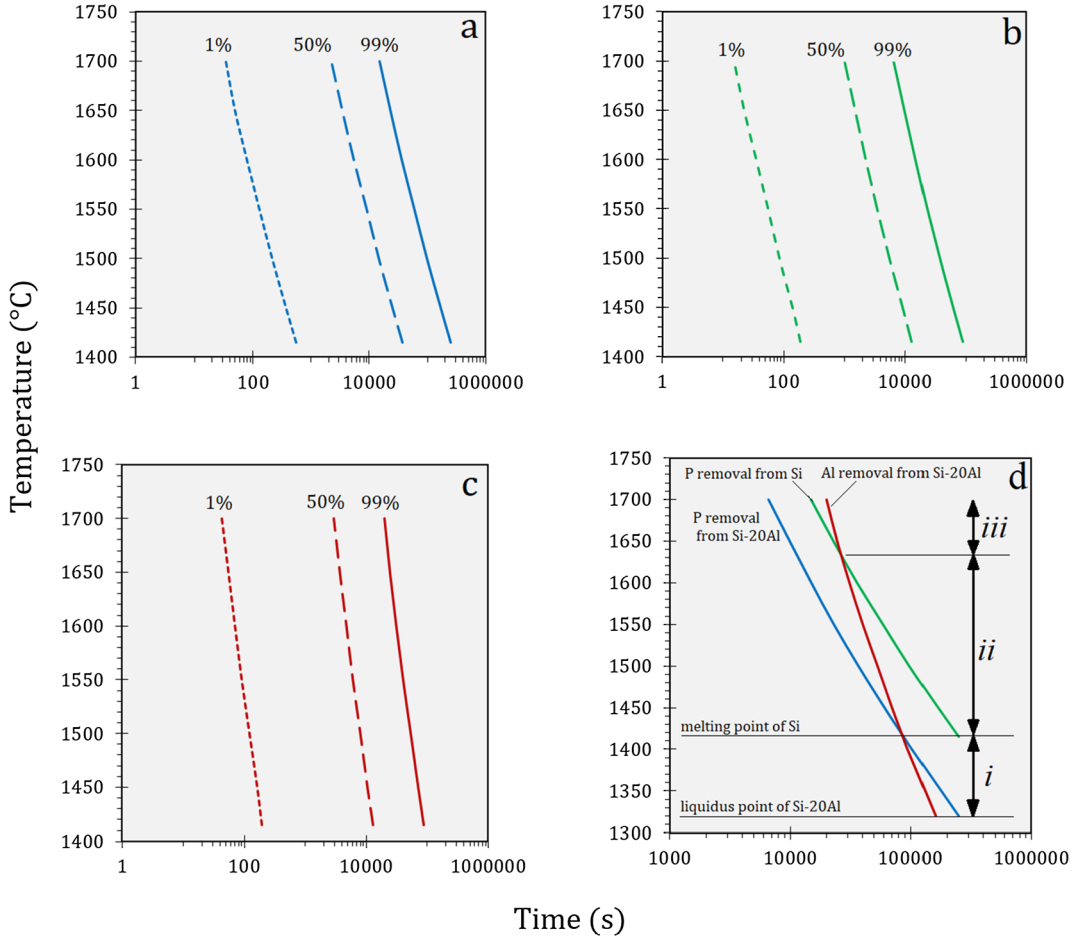

Fig. 4. IT diagrams of P and Al removal from Si and Si-20Al melts. (a): P removal from Si melt, (b): P removal from Si-20Al melt, (c): Al removal from Si-20Al melt, (d): A comparison of the 99% removal curves for P and Al removal from Si and Si-20Al melts.

where N_i denotes the molar flux of evaporation for element i from the melt. $p_i^{e.s}$ is the equilibrium vapor pressure of element i and p_i^{bp} is called the *back pressure* of i at the melt surface and shows the real partial vapor pressure of the i in the chamber, if there is no pressure profile above the melt. In other words, the p_i^{bp} would be almost zero if there is a perfect vacuum condition in the chamber. Thus, the HKL model for evaporation is thermodynamics model which deals with the evaporation from the melt surface and does not consider the diffusion in the melt and diffusion in the gas phase on top of the melt. Further information about HKL equation and its components can be found in [27,58–60]. In this paper we discuss two approaches to deal with the HKL equation. First, we start with the *Mass balance approach* developed by Olette [61] and is discussed in Section 4.1. Consequently, we continue by developing a new numerical stepwise solution approach in Section 4.2.

4.1. Mass balance approach to HKL equation

Michel Olette [61] presented the mass balance approach to HKL equation in 1961 for the evaporation of a minor elements from binary metal systems. What makes this method interesting is the possibility to investigate the evaporation of elements relative to each other in the vacuum refining process and independent of time. Here we update and expand this approach for a ternary system of i-j-l constituents with rewriting the HKL Eq. (7) as follows:

$$J_i\left[\frac{g}{m^2.\ s}\right] = \frac{dm_i}{A.\ dt} = 0.04375 p_i^e \sqrt{M_i T^{-1}} \tag{8}$$

where J_i is the mass flux of evaporation for element i, the p_i^e denotes the equilibrium pressure of element i in the gas phase and at the melt surface, which corresponds to the surface concentration of i. In order to obtain p_i^e, we can apply the relationship of Gibbs free energy change for the evaporation of species i from the melt as follows:

$$\underline{i} = i_{(g)} \tag{91}$$

$$\Delta G_{\underline{i}}^{ev} = -RTln\left(\frac{\varphi_i}{a_i}\right) \tag{92}$$

where $\Delta G_{\underline{i}}^{ev}$ denotes the Gibbs free energy change for the evaporation of $\underline{i}$, the $\underline{i}$ and $i_{(g)}$ are denoting the dissolved and gaseous forms of element i, respectively. The parameter φ_i is the fugacity of i at the gas phase, and a_i is the activity of element i in the melt. The φ_i and a_i can be defined through the following equations;

$$\varphi_i = \frac{p_i^e}{p^\circ_i} \tag{10}$$

$$a_i = x_i^m \cdot \gamma_i \tag{11}$$

where γ_i and x_i^m denote the activity coefficient and molar fraction of element i in melt, respectively. Parameters p°_i and p_i^e denote the standard vapor pressure and the equilibrium vapor pressure of element i, respectively. Now p_i^e can be calculated by inserting Eqs. (10) and (11) into Eqs. (9–12) as follows:

$$p_i^e\ [\mathrm{Pa}] = \gamma_i \cdot x_i^m \cdot p^\circ_i \cdot \exp\left(\frac{-\Delta G_{\underline{i}}^{ev}}{RT}\right) \tag{12}$$

where γ_i and x_i^m denote the activity coefficient and molar ratio of element i in melt, respectively. This equation shows that the p_i^e is a function of the x_i^m. It should be mentioned that during the vacuum refining process, the x_i^m changes over time due to the evaporation of melt constituents and this makes the x_i^m to be time dependent. In addition, the activity coefficient of i (γ_i) would be a function of time as x_i^m is changed due to evaporation. Here, by considering the mass balance for the elements in a ternary system i-j-l, we can calculate the molar fraction of i in melt at time t, $x_{i,t}^m$, through the following equation:

$$x_{i,t}^m\ [mol] = \frac{\frac{m_{i,0} - m_{i,t}}{M_i}}{\left[\frac{m_{i,0} - m_{i,t}}{M_i} + \frac{m_{j,0} - m_{j,t}}{M_j} + \frac{m_{l,0} - m_{l,t}}{M_l}\right]} \tag{13}$$

where $m_{i,0}$ and $m_{i,t}$ denote the initial mass and the evaporated mass of elements i, j, l until time t, respectively. By inserting Eq. (13) into Eq. (8), the mass flux of evaporation (Eq. (7)) can be re-written as follows:

$$J_i\left[\frac{g}{m^2.\ s}\right] = \frac{dm_i}{A.\ dt} = 0.04375 \gamma_i p^\circ_i \sqrt{M_i T^{-1}} \frac{\frac{m_{i,0} - m_{i,t}}{M_i}}{\left[\frac{m_{i,0} - m_{i,t}}{M_i} + \frac{m_{j,0} - m_{j,t}}{M_j} + \frac{m_{l,0} - m_{l,t}}{M_l}\right]} \tag{14}$$

In a ternary system of *i-j-l* if one or more constituents are volatile, the activity coefficient of constituents would be time dependent since γ_i is a function of the concentration of various constituents. Now we can see that there are two terms (p_i^e and γ_i) that depend to the molar fraction of element i, hence they would be time dependent which makes it difficult to solve Eq. (8) by the integration method. Here, the mass balance approach developed by Olette [61] can be applied to investigate the evaporation of melt constituents relative to each other, and by writing Eq. (8) for two arbitrary elements i and j and dividing them the following equation can be achieved;

$$\frac{dm_i}{dm_j} = \left[\frac{\gamma_i \cdot p^\circ_i \cdot \sqrt{M_j}}{\gamma_j \cdot p^\circ_j \cdot \sqrt{M_i}} \exp\left(\frac{\Delta G_{\underline{j}}^{ev} - \Delta G_{\underline{i}}^{ev}}{RT}\right)\right] \cdot \left(\frac{m^\circ_i - m'_i}{m^\circ_j - m'_i}\right) \tag{15}$$

If we consider:

$$\alpha_{i-j} = \frac{\gamma_i p^\circ_i \sqrt{M_j}}{\gamma_j p^\circ_j \sqrt{M_i}} \exp\left(\frac{\Delta G_{\underline{j}}^{ev} - \Delta G_{\underline{i}}^{ev}}{RT}\right) \tag{16}$$

By defining α_{i-j} as the *volatility coefficient* of i from j, Eq. (15) can be rewritten as follows:

$$\frac{dm'_i}{dm'_j} = \alpha_{i-j} \cdot \left(\frac{m^\circ_i - m'_i}{m^\circ_j - m'_j}\right) \tag{17}$$

This equation presents the ratio of the evaporation rate of i to that for j. It should be mentioned the m'_i and m'_j are variable and integration of Eq. (17) leads to:

$$m'_i = -\left[\frac{m^\circ_i}{(m^\circ_j)^{\alpha_{i-j}}}\right] \cdot (m^\circ_j - m'_j)^{\alpha_{i-j}} + m^\circ_i \tag{18}$$

By rearranging of this equation, we can calculate the evaporated fraction of i as a function of the evaporated fraction of j as follows:

$$\frac{m'_i}{m^\circ_i} = 1 - \left[1 - \frac{m'_j}{m^\circ_j}\right]^{\alpha_{i-j}} \tag{19}$$

The left side of this equation ($\frac{m'_i}{m^\circ_i}$) presents the fraction of the evaporated i and the division in the right side ($\frac{m'_j}{m^\circ_j}$) presents the evaporated fraction of element j. Eq. (19) is independent of time and can be applied to judge about the feasibility of removing of element i from the melt by vacuum refining, and also determine mass losses for reaching target compositions. The important point to emphasize here is that the volatility coefficient, Eq. (12), is a variable during the vacuum refining, while Ollete [61] considered it as a constant. Fig. 4a presents the mass loss of element i as a function of mass loss of element j plotted for various volatility coefficients of i from j (α_{i-j}). Fig. 5a shows that three scenarios can take place in evaporation of i from the melt according to the magnitude of the α_{i-j} as follows:

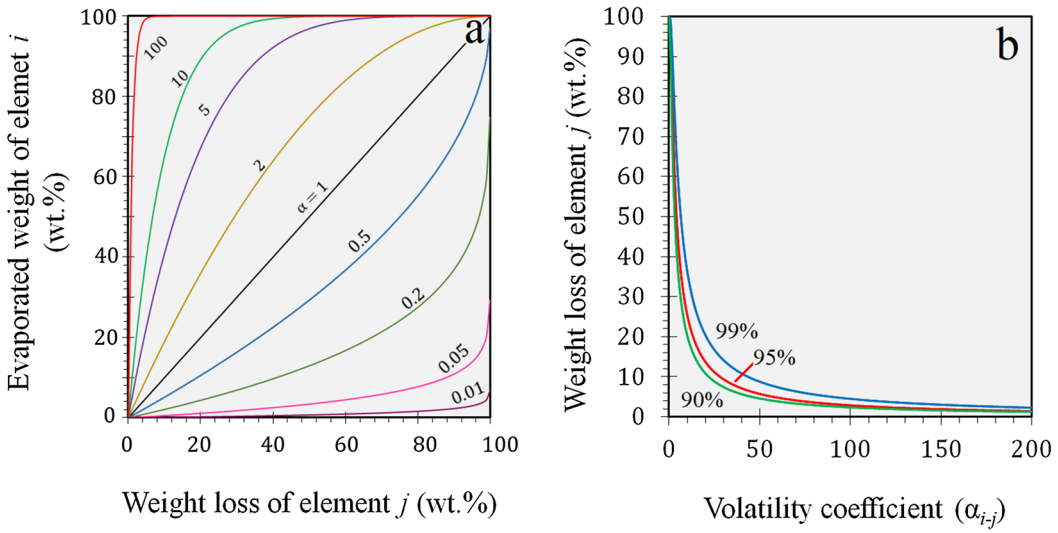

Fig. 5. (a): the volatility coefficient chart, representing the evaporated mass of solute *i* as a function of evaporated mass of solvent *j* at various alpha numbers. (b): The curves represent the weight loss of solvent *j* for removal of 90, 95, and 99% of the solute *i* as a function of α-number.

a. $\alpha_{i-j} > 1$; evaporation of species *i* dominates on evaporation of species *j*.
b. $\alpha_{i-j} = 1$; the same content of *i* and *j* evaporate from the melt.
c. $\alpha_{i-j} < 1$; evaporation of element *j* dominates on evaporation of element *i*.

Thus, the vacuum refining can be feasible for the separation of *i* from *j*, only if the $\alpha_{i-j} > 1$. the separation of *i* from *j* intensifies at higher magnitudes of the α_{i-j}. This is shown better in Fig. 5b, where the weight loss of the element *j* (here we consider the j as the constituent that we like to keep it in the melt and should be less volatile compared to *i*) is plotted as a function of the separation coefficient (α_{i-j}). Fig. 5b shows that for removing a specific amount of species i (e.g. 90%) from the melt, the mass loss of *j* reduces by increasing the volatility coefficient α_{i-j}. In addition, it is clear from Fig. 5b that when a greater degree for the removal of *i* is demanded the curves shift upward indicating that more mass loss of *j* would happen. It must be mentioned that in the ternary system of *i-j-l*, with the application of the same method for comparing evaporation of *i* with *j*, one can calculate the α_{l-j} and α_{i-l} to compare the evaporation of *l* with *j* and *i* with *l*, respectively.

To outline about removal of P from Si-Al alloy and compare it with P removal from Si alloy, we need to calculate the volatility coefficient of P from Si (α_{P-Si}). The evaporation of P and other volatile species from Si were investigated with this method before in the literature [34,61]. However, in all the previous studies the melts were considered as infinite dilute solution of i in j (like P in Si). In this case the activity coefficient of *i* (minor element) could be calculated from the Henry's law ($x_i \rightarrow 0$; $\gamma_i \rightarrow \gamma^{\circ}_i and \gamma^{\circ}_i is constant$) and the activity coefficient of *j* could be considered as unity according to Raoult's law ($x_i \rightarrow 1$; $\gamma_i \rightarrow 1$) during the whole process. That approach works well if a solution shows Henrian or ideal behavior and the activity coefficients of the constituents in the solution are constant. However, when the solution is not dilute and is not Raoultian, the activity coefficient and the molar fraction of the constituents are both changed over time due to the evaporation of the melt constituents with different rates. Thus, in the ternary *i-j-l* alloy, the elements *i*, *j* and *l* evaporate and this leads to the change of x_i, x_j and x_l in the melt over time. Removal of P from the Si-Al alloy is a good example for this case where the melt composition changes continuously, mainly due to Al evaporation (P concentration change is negligible). This causes correspondingly the changes of the activity coefficients of the melt constituents over time. Fig. 6a represents the γ_{Al} and γ_{Si} as a function of x_{Al} in the melt obtained by considering Eq. (16), we need the ΔG^{ev}_P and ΔG^{ev}_{Si} to calculate the α_{P-Si} and α_{Al-Si}, and they can be calculated through the following equations:

$$\Delta G^{ev}_i = \Delta G^{ev}_i - \Delta \bar{G}_i \quad (20)$$

where ΔG^{ev}_i denotes the partial molar Gibbs free energy change for evaporation of solute *i*, ΔG^{ev}_i denotes molar Gibbs free energy change for evaporation of pure *i*, and $\Delta \bar{G}^{M}_i$ denotes the molar Gibbs free energy change for mixing *i*.

The $\Delta \bar{G}_{Si}$ and $\Delta \bar{G}_{Al}$ for mixing Si and Al in the Si-Al alloy is also presented in Fig. 6(b–d) present ΔG^{ev}_{Si} and ΔG^{ev}_{Al}. In addition, the relationships of ΔG^{ev}_{Si} and ΔG^{ev}_{Al} for Si and Al can be found in the Table A1. Now we can insert the information presented in Table A1 into Eq. (16) to calculate the volatility coefficients α_{P-Si} and α_{Al-Si}. It should be mentioned that the γ_P in Si-Al melts are not studied and the interaction of Al with P (ε^{Al}_P) in Si cannot be found in literature, we assumed the γ_P in Si-Al melt to be the same as in Si melt and we applied the results of Zaitsev [54].

By employing Eq. (16), the α_{P-Si} and α_{Al-Si} are calculated as a function of Al content in the Si-Al melts and the results are plotted in the Fig. 7. This figure shows that the curves of α_{P-Si} and α_{Al-Si} shift down when the temperature of the process is increased. This is because of the increase of the standard vapor pressure of Si at higher temperatures, meaning more Si evaporation simultaneously with Al and P at higher temperatures. Since the α_{P-Si} and α_{Al-Si} can be calculated, the evaporation of P and Al from Si by plotting Eq. (19) can be studied. For this purpose, we applied the equations of α_{P-Si} and α_{Al-Si} presented in Table A2 and the results are presented in Fig. 8(a) and (b). This figure shows that by increasing the temperature both curves of P and Al shift downward, leading to increase the Si loss. Fig. 8 shows that both Al and P evaporate intensively during the refining process, and these curves can be used to calculate the amount of Al and Si loss for the removal of a specific amount of P from the melt.

The mass balance approach presented in this section was expanded for a ternary system, however, it can be expanded for a system consisting of four or more constituents as well. The discussions presented in this section showed that we can investigate the evaporation of melt constituents by comparing their rates of evaporation and we can calculate the amount of solvent loss for removing a specific amount of the solute as is shown in Fig. 5b. However, it is not efficient to predict the time of the vacuum refining process. To further make a more flexible model, including the process time, a numerical approach is done in Section 4.2.

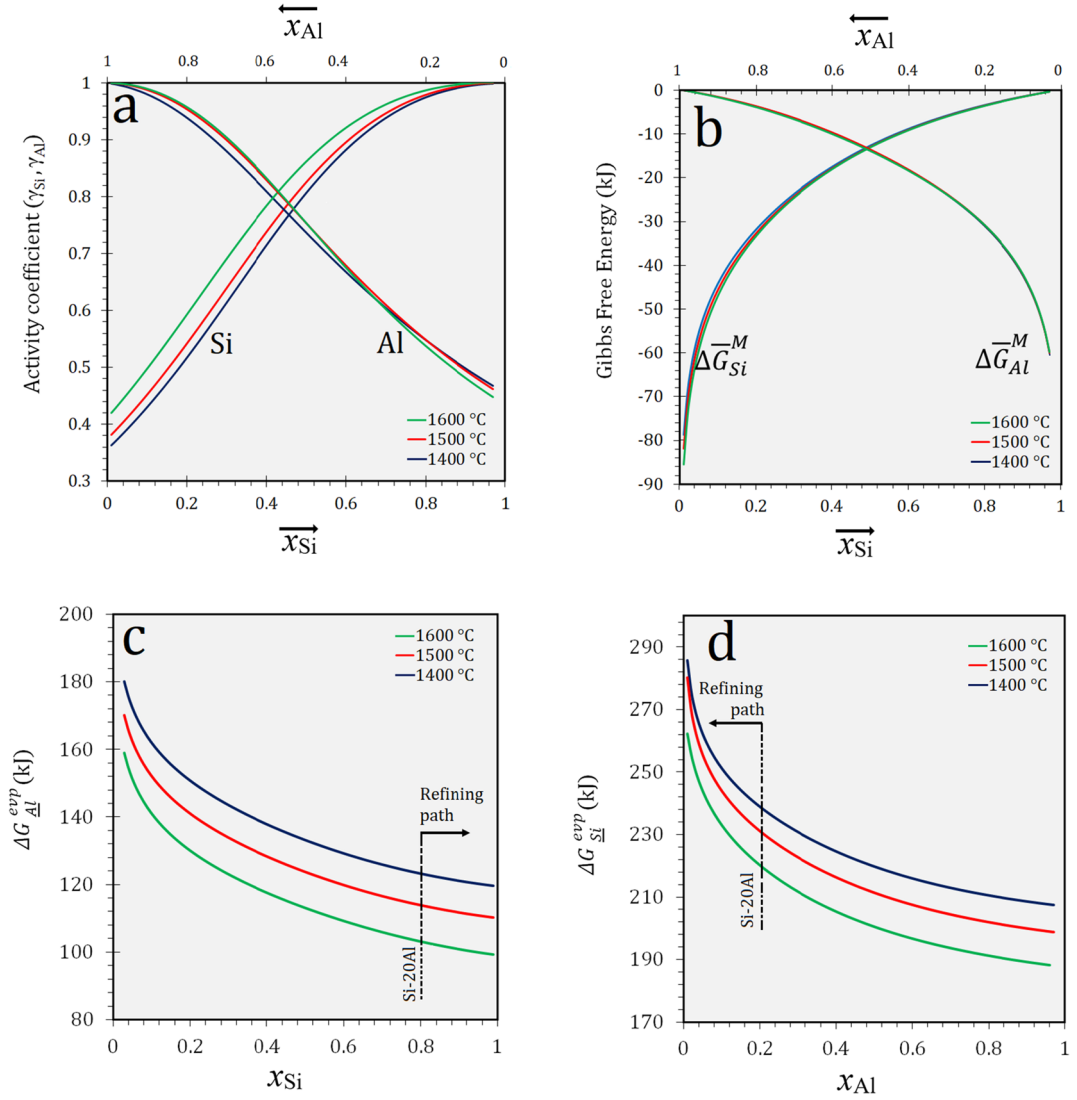

Fig. 6. Thermodynamics properties of Si-Al system at various temperatures (a): the activity coefficients of Si and Al, (b): Gibbs free energy of mixing for Si and Al in the Si-Al solution. (c): Partial Gibbs free energy of the evaporation of Al from Si-Al melts (ΔG^{evp}_{Al}), (d): Gibbs free energy of the evaporation of Si from Si-Al melts (ΔG^{evp}_{Si}).

4.2. Numerical approach to HKL model

In this section we present a numerical kinetic approach using the HKL equation and calculate the mass evaporation rate of volatile constituents in the vacuum refining of a ternary system such as molten Si-Al-P melts. Eq. (7) has been applied to investigate the evaporation of an infinitive dilute solution of *i* from the solvent j, as previously applied for binary systems like Si [10,62,63] and copper [27,32,33,58,64]. In these studies, the chemical evaporation flux is a linear function of the concentration as described previously for P evaporation from the dilute solutions of P in Si-P melt [10]. However, for a ternary system like Si-Al-P whose composition changes during the process, and the activity coefficient of the species are not constant, the chemical evaporation flux is not any more a linear function of the composition. In other word, the former literature work equations can be applied directly to study evaporation from dilute solutions and ideal solutions, while considering the change of the activity coefficient along with composition change is more reliable for wide composition ranges. The un-linear dependence of evaporation flux on composition is actually hidden in γ_i in Eq. (12) and therefore we need to develop a numerical solution for this condition.

For kinetic modeling, we start with the calculation of the equilibrium pressure of the melt's constituents (p^e_{Si}, p^e_{Al}, p^e_P) for the initial composition by applying the Eqs. (9–12). In the case of Si-Al-P melts, one can find the required thermodynamics data of Al and Si from Fig. 6 and Table A1. However, since no thermodynamics data about the partial pressure of the P in equilibrium with Si-Al-P melts is found, here we apply the pressure of phosphorus in equilibrium with Si-P melt, which has been experimentally investigated by Zaitsev [54,65]. It should be mentioned that this assumption could lead to some errors, which are discussed later. As it was mentioned, the *back pressure* of element *i*, represents the partial pressure of the *i* in the chamber and it can be calculated through the following equation:

$$p_i^{bp} = x_i^v \cdot p_t \tag{21}$$

where p_t and the x_i^v are the total pressure of the chamber and molar fraction of species *i* in the gas phase, respectively. Assuming no concentration profile in the melt, inserting the Eqs. (20 and 9–12) in Eq. (7), we obtain:

$$J_i = \frac{x_i^m \cdot \gamma_i \cdot p^{\circ}_i - x_i^v \cdot P_t}{\sqrt{2 \cdot \pi \cdot M_i \cdot R}} \tag{22}$$

Eqs. (21) and (22) indicate that when there is not a perfect vacuum

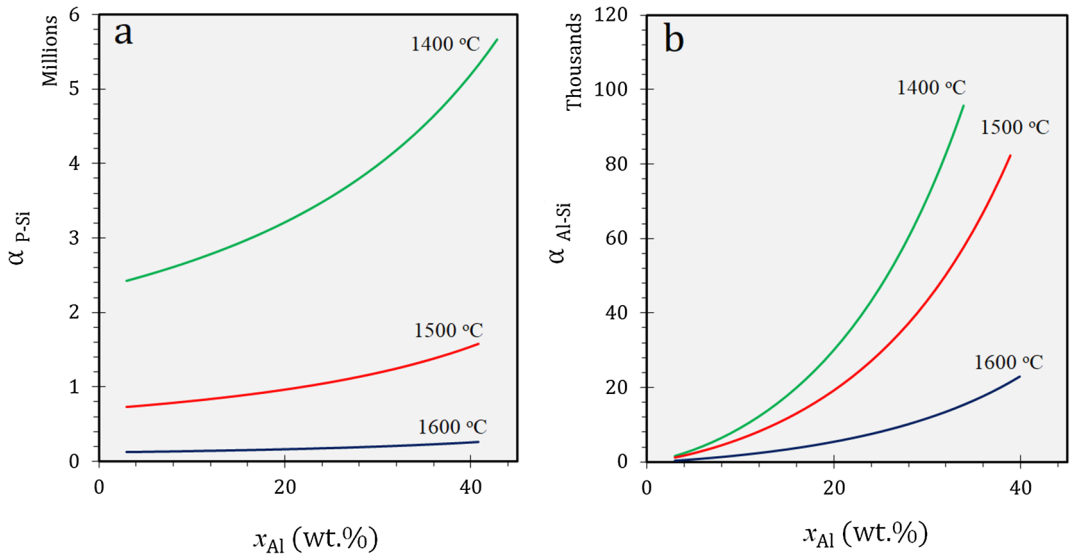

Fig. 7. The calculated volatility coefficients of P and Al from the Si-Al melts as a function of Al content in at various temperatures: (a) P from Si (α_{P-Si}), (b): Al from Si (α_{P-Si}).

in the chamber the evaporation flux of element i is lower. The numerical approach that is presented in this section is based on calculating the concentration of the constituents of the melt at any time t regarding to the total evaporated masses of the components from initial time ($t = 0$). These total evaporated masses are calculated by discretizing the Eq. (22) in sequences after short interval times from t to $t + \Delta t$ and then integration from time zero to time t. A flowchart is presented in Fig. 9 to describe the algorithm of this stepwise solution approach. The corresponding equations of this procedure are presented in Table 3, and the steps of calculations are summarized as follows:

a. Input the initial mole of each constituent in solution at $t = 0$.
b. Calculate the molar ratio of all constituents in the melt (x_P^m, x_j^m, x_l^m).
c. Calculate the activity coefficient of Al and Si as a function of their concentrations in the melt and the vapor pressure of phosphorus, for a constant temperature.
d. Calculate the molar flux of evaporation for all constituents for the given concentrations
e. Obtain the moles of evaporated constituents from the surface within interval Δt, here we consider interval of one second.
f. Calculate molar fraction of the evaporated constituents in the gas phase.
g. Calculate the *back pressure* of each constituent by considering the assumed pressure in the chamber and applying Eq. (21).
h. Calculate the amount of the remained moles of constituents in the melt up to time $t_0 + \Delta t$.
i. Enter to the next step restart from step b and calculate the concentrations in the melt for step $t_0 + 2\Delta t$.
j. Frequent calculations for n times from step b to determine remained components in the melt to time t, where $t = n\Delta t$.

It should be mentioned that by applying this algorithm one can investigate the effect of chamber pressure on evaporation by considering various pressures as p_t in Eq. (21) and step g of the flowchart. This kinetic modeling approach is flexible and we can apply it to investigate the effect of various parameters like temperature, chamber pressure, melt geometry, and melt composition on the evaporation of the melt constituents. This was done for vacuum refining of Si-Al-P and Si-P as discussed in the following sections.

4.3. Verification of numerical approach to HKL

4.3.1. Effect of pressure and temperature

The P and Al evaporation from the Si-20Al melt at various melt

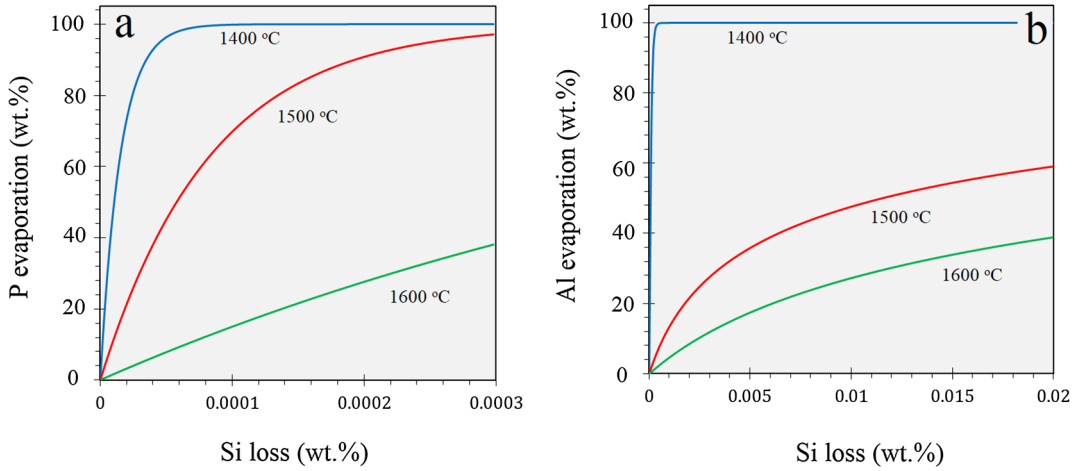

Fig. 8. The α-charts prepared for P and Al removal from Si-Al melts at various temperatures; (a): α-chart of P evaporation from Si-Al melt, (b): α-chart of Al evaporation from Si-Al melts.

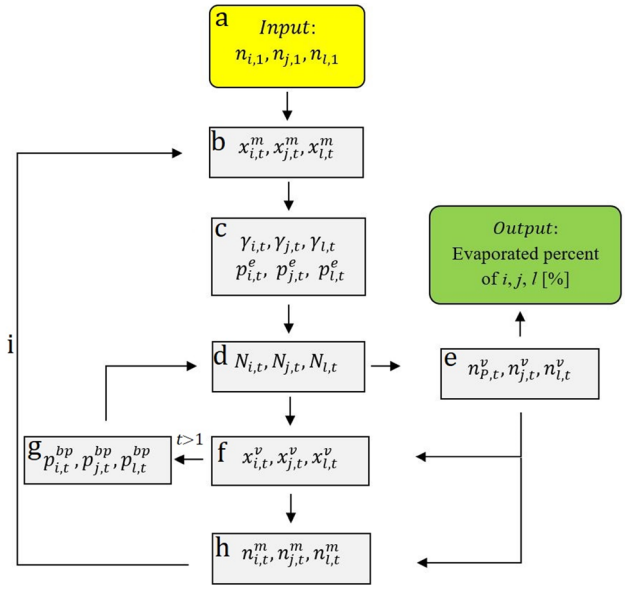

Fig. 9. The flowchart describing the algorithm for the developed numerical solution.

pressures is calculated by the present numerical model and the results are presented in Fig. 10. The experimental results presented in Table 1 are also marked on the Fig. 10 as well. This figure shows that the calculated curves fit fairly well with the obtained experimental data. Fig. 10 shows that the highest mass loss for each element takes place at the perfect vacuum condition in the chamber and as the pressure in the chamber increases the weight loss curves shift downwards for both P and Al species. Obviously, the maximum rate and extent of evaporation for each constituent takes place at the perfect vacuum conditions in the chamber where the back pressure is zero. However, in practice, it is not possible to reach perfect vacuum, thus the points of the experimental results must be always at lower position than the theoretical curve for perfect vacuum condition. Fig. 10 shows this expectation for Al evaporation, while in the case of P the experimental data are slightly above the curve of perfect vacuum condition. This may be due to the inaccurate thermodynamic data we considered for equilibrium P pressure calculation in dilute solutions of P in Si-Al-P melts. As we mentioned before, there is no information about the partial pressure of the P in equilibrium with dilute P solutions in Si-Al-P alloy and we used the pressure of P in equilibrium with dilute P solutions in Si-P melts from literature [54,65]. It should be mentioned that if Al has a positive interaction with the P in Si melt, then the P pressure in Si-Al-P alloy would be greater than P pressure in Si-P melt. Thus, by inputting

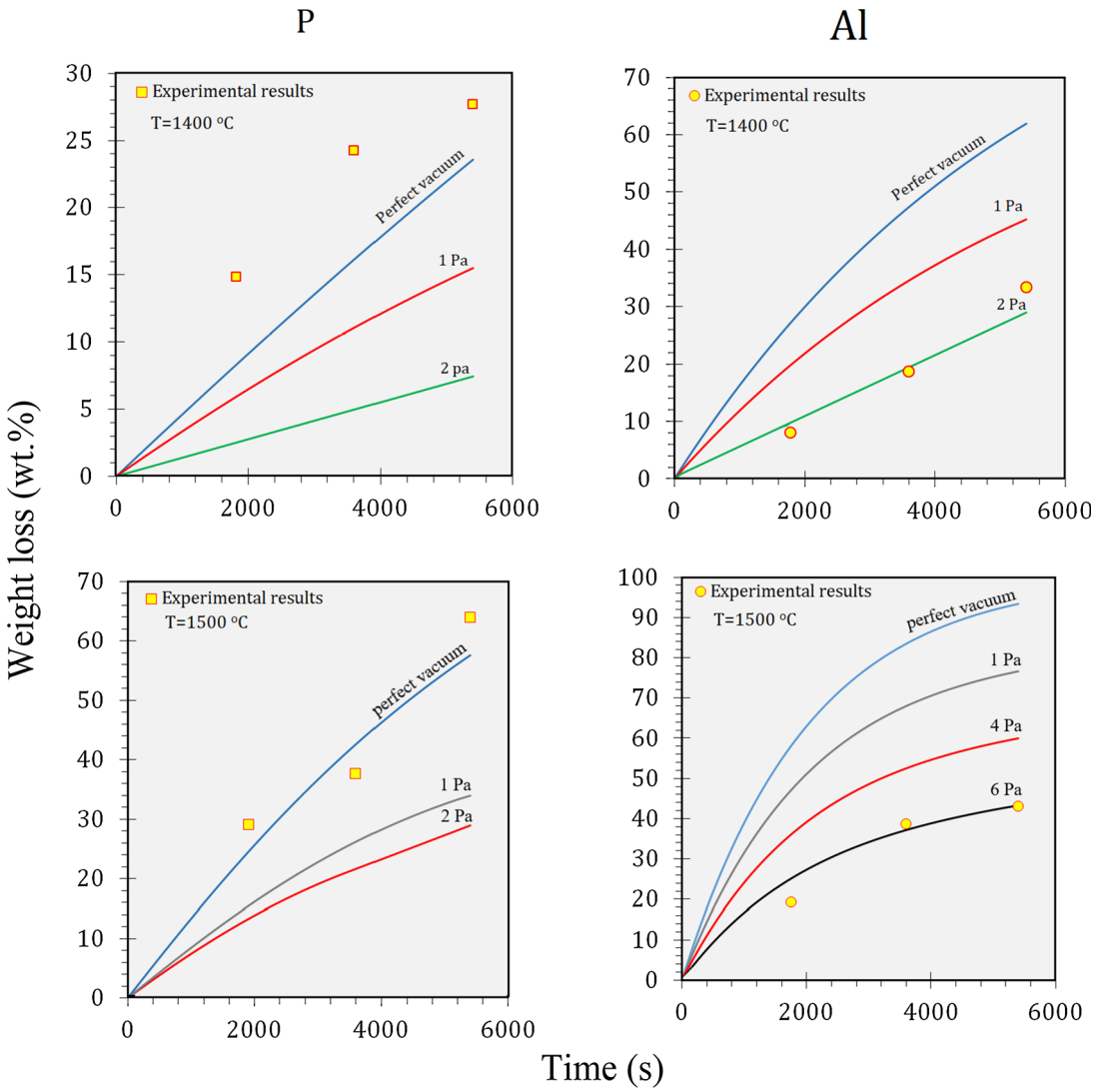

Fig. 10. The P and Al evaporative mass losses from Si-20Al melt as a function of time at 1400 °C and 1500 °C and various chamber pressure. The points on the figures represent the experimental results.

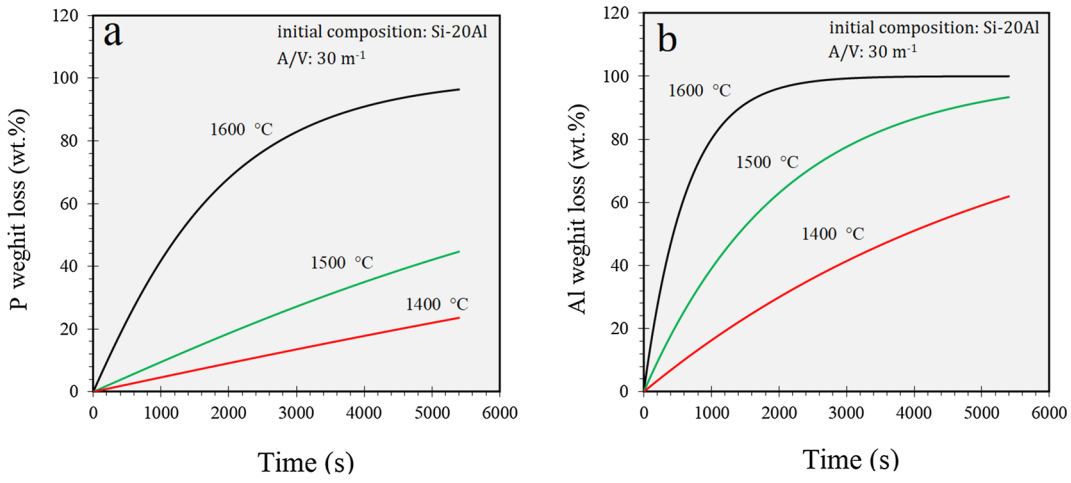

Fig. 11. The effect of temperature on the evaporative mass losses of P ad Al in vacuum refining process calculated by the present model. All curves are for the perfect vacuum condition from initial Si-20 wt%Al melt composition. (a): P evaporation, (b): Al evaporation.

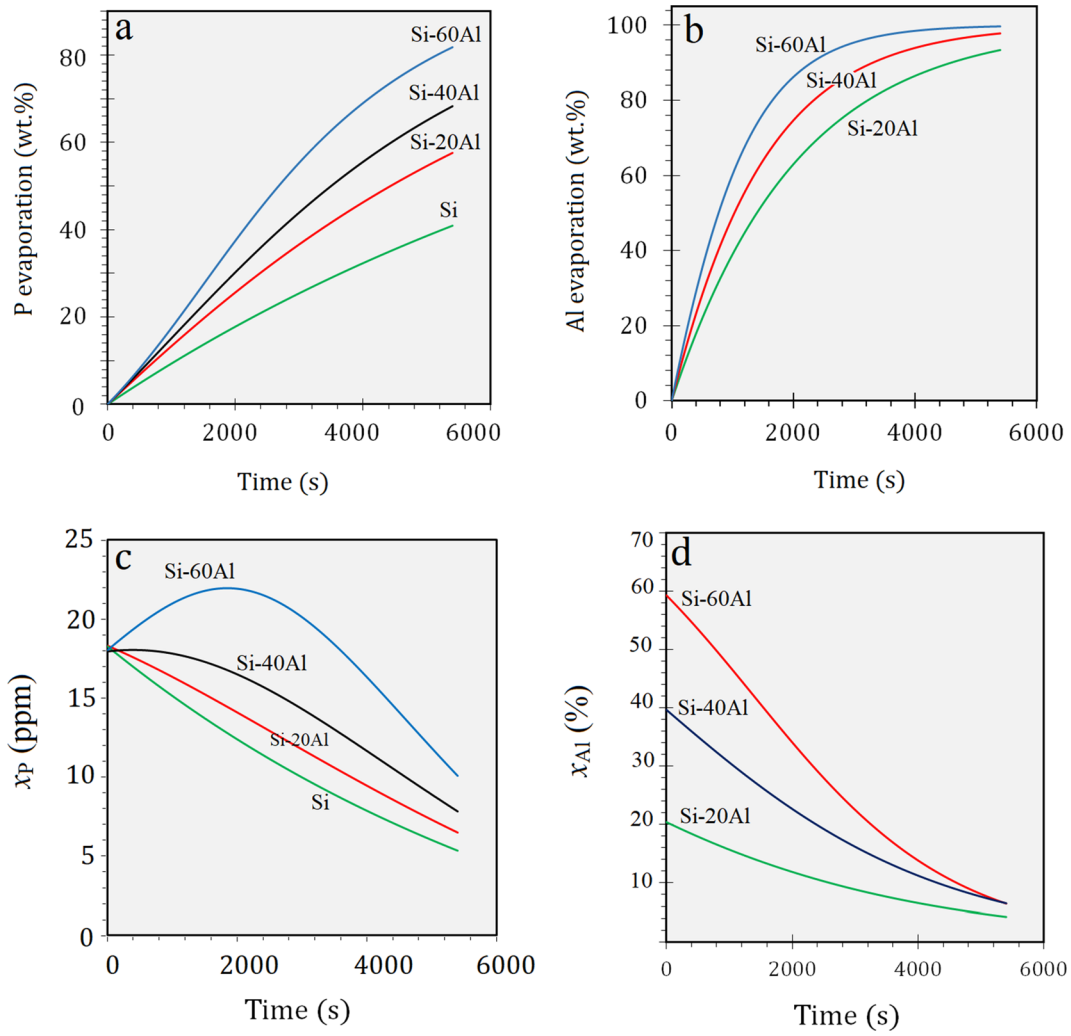

Fig. 12. The effect of initial composition of the Si-Al-P melt (Al content) of the P evaporation (a) and Al evaporation (b) from the melts under perfect vacuum conditions.

correct data, the curves related to P evaporation in Fig. 10 shift up toward the experimental results.

Fig. 11 depicts the effect of temperature on the evaporation of P and Al calculated by the numerical approach (presented in Figure) to HKL model. This figure shows that temperature has a significant effect on the rate of evaporation for Al and P and they evaporate with a considerably faster kinetics at higher temperatures. Fig. 11 shows the shape of the curves of evaporation changes from linear to parabolic by increasing

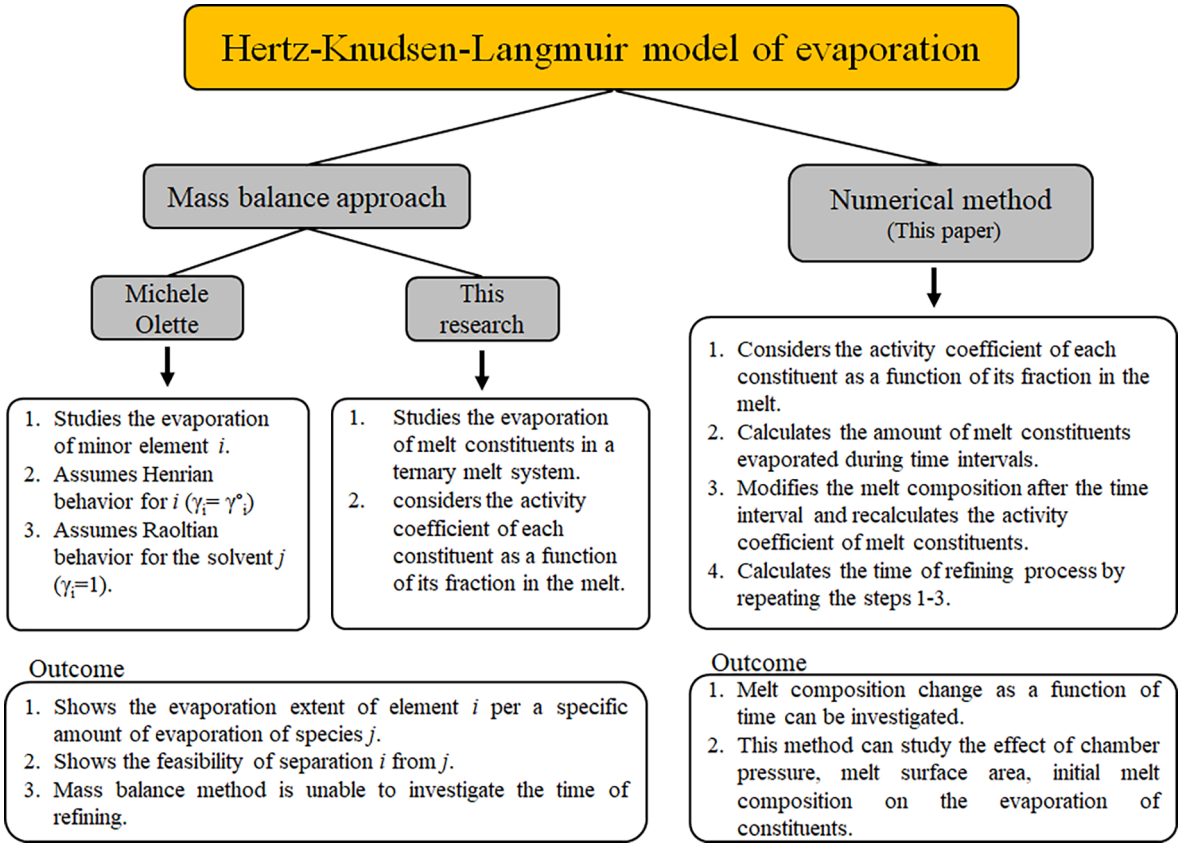

Fig. 13. A comparison between the features of the mass balance approach and the numerical approach to study the vacuum refining process.

the temperature from 1400 °C to 1600 °C.

4.3.2. Effect of initial melt composition

The effect of the initial Al content on the rate of P and Al removal are shown in Fig. 12, for perfect vacuum condition and at 1500 °C. As we see, by increasing the initial Al content the curves for P and Al shift toward higher positions (Fig. 12a and b). Comparing Fig. 12(a and b), we can see higher extents of Al evaporates from melt than P in the same melt compositions. The change of molar fraction of P and Al in the melt (x_P^m and x_{Al}^m respectively) are presented in Fig. 12(c and d). Fig. 12c shows that the P fraction in the melt decreases by the time of vacuum refining, but x_P^m shifts to higher positions by increasing the Al content. As shown in Fig. 12 (a and b), Al evaporation is greater than P evaporation leading the x_P^m to grow. In addition, Fig. 12c shows when Al content is 60%, the x_P^m first rises from 0.0018% up to 0.022% in 1800 s of vacuum refining and subsequently drops. Comparing Figs. 12c with d, it reveals that the Al content has decreased from 60% to about 40% within the same time. This means that about 20% of the melt (mainly Al) is evaporated from melt which causes the simultaneous x_P^m increase. Shifting of x_P^m to higher positions by the Al is in contract with the experimental results we presented in Fig. 2, where we showed P removal from Si-20Al melt is greater than Si melt. This can be explained by the mechanisms that Al affects P evaporation as follows:

a. The effect of Al evaporation on the molar fraction of P in the melt (x_P^m); it is noticed that Al is a major constituent in the ternary system of Si-Al-P, therefore, as Al leaves the melt, the fraction of other elements would increase in the melt. Considering the Eqs. (7) and (12), the higher the fraction of species *i*, the higher the vapor pressure and evaporation flux of *i*.
b. The effect of Al on the vapor pressure of P; the presence of Al in the melt can accelerate the P evaporation if Al had a positive interaction (ε_P^{Al}), coefficient with P, which makes the γ_P, and consequently the vapor pressure of P to increase. Considering the Eqs. (7) and (12), the higher the vapor pressure of P the higher the evaporation flux of P evaporation.
c. Effect of Al on the fluid properties of the melt, like surface tension, viscosity, and diffusion coefficient of P in the Si.

As we mentioned earlier there is no data about the interaction of Al with P in Si melts and the curves developed by the present model are based on the thermodynamic data available for P in Si-P melt, in other word the curves are developed with the assumption that Al has no interaction with P ($\varepsilon_P^{Al} = 0$). As Al is being applied as the impurity getter in the solvent refining of Si, the ε_P^{Al} is expected to (and must) be negative in the solvent refining process. However, the studying temperature and the alloy composition in this research is different with the conditions of solvent refining process and ε_P^{Al} could be different at high temperatures where only liquid phase is stable.

The results presented in the Sections 4.1 to 4.2 showed that vacuum refining can be studied by mass balance model (Section 4.1) or the numerical model (Section 4.2), based on HKL theory. Fig. 13 compares the capabilities of these two models to study vacuum refining process of molten alloys. The mass balance approach (developed by Olette [61]) is mainly discussing the feasibility of removing a volatile element from the melt, while the numerical approach developed in this work for the case of Si-Al-P system is a more global model and can be applied to investigate the effect of all process parameters chamber pressure, melt geometry, temperature, and refining time of the process.

5. Conclusions

Experimental results: Vacuum refining of Si-20 wt%Al alloy was investigated experimentally at 1400 °C and 1500 °C in this research, leading to the following results:

1. Vacuum refining of P is feasible at temperatures lower than the melting point of Si in the Si-Al melts.
2. Phosphorus in dilute solutions could be removed faster from Si-20wt.%Al melts compared to Si melt.
3. An apparent activation energy for P evaporation from Si-Al alloy (E_P) was determined as 249.4 kJ mol^{-1}, which may indicate that Al addition to the silicon melt reduces the apparent activation energy by 8.64% compared to silicon melt.

Modeling results: The Hertz-Knudsen-Langmuir theory for evaporation was applied to study the simultaneous evaporation of Al and P from the ternary system of Si-Al-P, using a mass balance approach and developing a numerical solution. The results are summarized as follows:

1. The numerical model is more flexible than the mass balance model with flexibility to include the vacuum refining process duration.
2. The applied mass balance approach in this study is applicable to study vacuum refining for all type of solutions in which the volatility coefficient can be a non-linear function of composition.
3. The P evaporation is accelerated with the increase of temperature, and initial Al content of the melt.
4. Al in Si-Al-P melts may have a positive interaction with P.
5. The numerical approach presented in this paper has superiority on the mass balance approach and can be applied to investigate the effect of various parameters such as: time, melt geometry, composition, and temperature.

Declaration of Competing Interest

Author declares that there is no conflicts of interest.

Acknowledgments

This work was financed by Norwegian University of Science and Technology (NTNU, Trondheim, Norway, project 70440577) and has been done in cooperation with the Research Centre for Sustainable Solar Cell Technology (FME SuSolTech) in Norway. The authors appreciate Erlend Lunnan Bjørnstad and Mengyi Zhu from NTNU for all the thermodynamics discussions contributed to this paper. The support from the *silicon materials* group from Elkem® Bremanger is acknowledged.

Appendix

The thermodynamics data required for doing the calculation presented in this paper are presented in the Table A1. The activity coefficients of Si and Al in the Si-Al binary alloys is calculated by FactSage 7.3 software and the process for calculating the ΔG_{Si}^{ev} and ΔG_{Al}^{ev} is explained by Eq. (20). The thermodynamic data of P in Si melt is obtained from literature [54,65]. In addition, Table A2 presents the relations of volatility coefficient curves of P and Al presented in Fig. 6.

Table A1
Thermodynamics data of the Si-Al binary system and dilute solutions of P in Si-P.

Element	Temperature (°C)	Activity coefficient of i (γ_i) Partial Gibbs energy for evaporation of element i, $\Delta\bar{G}_i^{ev}$ (J mol^{-1})
Si	1600	$\gamma_{Si} = 0.9517x_{Si}^4 - 2.719x_{Si}^3 + 1.9069x_{Si}^2 + 0.4958x_{Si} + 0.3617$ $\Delta G_{Si}^{ev} = -19962\ln(x) + 187526$
	1500	$\gamma_{Si} = 1.0827x_{Si}^4 - 2.5879\,x_{Si}^3 + 1.3735x_{Si}^2 + 0.72x_{Si} + 0.4143$ $\Delta G_{Si}^{ev} = -19280\ln(x) + 198309$
	1400	$\gamma_{Si} = 1.0235x_{Si}^4 - 2.7277x_{Si}^3 + 1.7597x_{Si}^2 + 0.5647x_{Si} + 0.3792$ $\Delta G_{Si}^{ev} = -18604\ln(x) + 207082$
Al	1600	$\gamma_{Al} = -0.4775x_{Al}^4 + 0.0281x_{Al}^3 + 0.6375x_{Al}^2 + 0.3658x_{Al} + 0.4387$ $\Delta G_{Al}^{ev} = -18040\ln(x) + 99979$
	1500	$\gamma_{Al} = -0.5558x_{Al}^4 + 0.2714x_{Al}^3 + 0.4383x_{Al}^2 + 0.3889x_{Al} + 0.4509$ $\Delta G_{Al}^{ev} = -18173\ln(x) + 110687$
	1400	$\gamma_{Al} = -0.7035x_{Al}^4 + 0.715x_{Al}^3 + 0.1105x_{Al}^2 + 0.4191x_{Al} + 0.455$ $\Delta G_{Al}^{ev} = 18357\ln(x) + 119976$
P	T	$\ln\gamma^{\circ}_{P} = 2.0805 - \frac{0.4766}{T}$ [65] $\Delta G_{Al}^{ev} = 347500–88.86\,T$ [54]

Table A2
The relations of volatility coefficients of Al and P from Si melt as a function of the Al content in the melt (x_{Al}) at various temperatures calculated in Fig. 7.

Temperature (°C)	Volatility coefficient
1400	$\alpha_{P-Si} = 2\times10^7x_{Al}^2 + 789754x_{Al} + 2\times10^6$, $\alpha_{Al-Si} = 2\times10^6x_{Al}^3 + 13451x_{Al}^2 + 59122x_{Al} + 1576$
1500	$\alpha_{P-Si} = 4\times10^6x_{Al}^2 + 303855x_{Al} + 733628$, $\alpha_{Al-Si} = 972086x_{Al}^3 + 61199x_{Al}^2 + 36425x_{Al} + 1183$
1600	$\alpha_{P-Si} = 681320x_{Al}^2 + 55887x_{Al} + 123976$, $\alpha_{Al-Si} = 224688x_{Al}^3 + 24460x_{Al}^2 + 10787x_{Al} + 391$

References

[1] R.N. Andrews, S.J. Clarson, Pathways to solar grade silicon, Silicon 7 (2015) 303–305, https://doi.org/10.1007/s12633-014-9235-x.
[2] G. Fisher, M.R. Seacrist, R.W. Standley, Silicon crystal growth and wafer technologies, Proc. IEEE (2012) 1454–1474, https://doi.org/10.1109/JPROC.2012.2189786.
[3] Shell, Shell Scenarios: Sky - Meeting the goals of the Paris agreement, (2018) 72. https://www.shell.com/energy-and-innovation/the-energy-future/scenarios/shell-scenario-sky.html.
[4] D.S. Philips, W. Warmuth, Photovoltaics report, Fraunhofer ISE. (2016) 1–43. doi:10.1016/j.compedu.2008.05.004.
[5] M. Tansgtad, Metal production in Norway, Akademika Publishing, Trondheim, 2013.
[6] E.J. Øvrelid, K. Tang, T. Engh, M. Tangstad, Crystal Growth of Silicon for Solar Cells, Springer, Berlin Heidelberg, Berlin Heidelberg, 2010, https://doi.org/10.1007/978-3-642-02044-5.
[7] A. Schei, J.K. Tuset, H. Tveit, Production of high silicon alloys, 1998.
[8] B.G. Fisher, M. Ieee, M.R. Seacrist, M. Ieee, R.W. Standley, Silicon crystal growth and wafer technologies, Proc. IEEE. 100 (2012) 1454–1474, https://doi.org/10.1109/JPROC.2012.2189786.
[9] A. Murgau, J. Safarian, solar silicon production through metallurgical route and REC solar advancements, Silicon Chem. Sol. Ind., Avolvær (2018) 18–192.
[10] J. Safarian, M. Tangstad, Vacuum refining of molten silicon, Metall. Mater. Trans. B. 43 (2012) 1427–1445, https://doi.org/10.1007/s11663-012-9728-1.
[11] N. Yuge, M. Abe, K. Hanazawa, H. Baba, N. Nakamura, Y. Kato, Y. Sakaguchi, S. Hiwasa, F. Aratani, Purification of metallurgical-grade silicon up to solar grade, Prog. Photovolt. Res. Appl. 9 (2001) 203–209, https://doi.org/10.1002/pip.372.
[12] N. Yuge, K. Hanazawa, K. Nishikawa, H. Terashima, Removal of phosphorus, aluminum and calcium by evaporation in molten silicon, J. Jpn. Inst. Met. 61 (1997) 1086–1093.
[13] S. Shi, P. Li, J. Meng, D. Jiang, Y. Tan, H.M.N. Ul, H.K. Asghar, Kinetics of volatile impurity removal from silicon by electron beam melting for photovoltaic applications, Phys. Chem. Chem. Phys. 19 (2017) 28424–28433, https://doi.org/10.1039/C7CP05080A.
[14] Ø.S. Sortland, M. Tangstad, Boron removal from silicon melts by H2O/H2 gas blowing : mass transfer in gas and melt, Metall. Mater. Trans. E. 1 (2014) 211–225, https://doi.org/10.1007/s40553-014-0021-x.
[15] J. Safarian, K. Tang, K. Hildal, G. Tranell, Boron removal from silicon by humidified gases, Metall. Mater. Trans. E. 1 (2014) 41–47, https://doi.org/10.1007/s40553-014-0007-8.
[16] A. Hosseinpour, L. Tafaghodi Khajavi, Slag refining of silicon and silicon alloys: a review, Miner. Process. Extr. Metall. Rev. 39 (2018) 308–318, https://doi.org/10.1080/08827508.2018.1459616.
[17] A. Hosseinpour, L. Tafaghodi Khajavi, Thermodynamics of boron removal in slag refining of Fe-Si alloy, J. Alloys Compd. 768 (2018) 545–552, https://doi.org/10.1016/j.jallcom.2018.07.246.
[18] Y. He, X. Yang, W. Ma, G. Lv, Y. Bao, S. Li, Z. Chen, Effects of silicon content on the separation and purification of primary silicon from hypereutectic aluminum–silicon alloy by alternating electromagnetic directional solidification, Sep. Purif. Technol. 219 (2018) 25–32, https://doi.org/10.1016/j.seppur.2018.10.033.
[19] J.L. Gumaste, B.C. Mohanty, R.K. Galgali, U. Syamaprasad, B.B. Nayak, S.K. Singh, P.K. Jena, Solvent refining of metallurgical grade silicon, Sol. Energy Mater. 16 (1987) 289–296, https://doi.org/10.1016/0165-1633(87)90077-3.
[20] B. Ban, T. Zhang, J. Li, X. Bai, X. Pan, J. Chen, S. Hadi Tabaian, Solidification refining of MG-Si by Al-Si alloy under rotating electromagnetic field with varying frequencies, Sep. Purif. Technol. 202 (2018) 266–274, https://doi.org/10.1016/j.seppur.2018.03.069.
[21] Z. Yin, A. Oliazadeh, S. Esfahani, M. Johnston, M. Barati, Solvent refining of silicon using nickel as impurity getter, Can. Metall. Q. 50 (2011) 166–172, https://doi.org/10.1179/000844311x12949307643551.
[22] J. Safarian, G. Tranell, M. Tangstad, Processes for upgrading metallurgical grade silicon to solar grade silicon, Energy Procedia (2012) 88–97, https://doi.org/10.1016/j.egypro.2012.03.011.
[23] L. Huang, H. Lai, C. Lu, M. Fang, W. Ma, P. Xing, X. Luo, J. Li, Evaporation behavior of phosphorus from metallurgical grade silicon via calcium-based slag treatment and hydrochloric acid leaching, J. Electron. Mater. 45 (2016) 541–552, https://doi.org/10.1007/s11664-015-4146-1.
[24] E. Enebakk, K. Friestad, R. Tronstad, C. Zahedi, C. Dethloff, Silicon feedstock for solar cells, 2548936, 2009.
[25] https://www.silicormaterials.com/, acessed 11 November 2019.
[26] E. Forines, A. Souto, T. Velasenko, A. Perez Vazquez, M. Tojeiro, M. Anoshenko, G. Varela, Performance of modules and solar cells made of 100% solar silicon purified by direct route, in: 35th Eur. Photovolt. Sol. Energy Conf. Exhib. Perform., 2018: pp. 473–475. 10.4229/35thEUPVSEC20182018-2AV.1.5%0A.
[27] R. Harris, W.G. Davenport, Vacuum distillation of liquid metals : part I. Theory and experimental study, M, r Metall. Trans. B. 13 (1982) 581–588.
[28] M.A. Van Ende, Y.M. Kim, M.K. Cho, J. Choi, I.H. Jung, A kinetic model for the Ruhrstahl Heraeus (RH) degassing process, Metall. Mater. Trans. B Process Metall. Mater. Process. Sci. 42 (2011) 477–489, https://doi.org/10.1007/s11663-011-9495-4.
[29] J. Szekely, S.D. Fang, Studies in vacuum degassing: mass and momentum transfer to gas bubbles rising in melts, the freeboard of which is evacuated, Met. Trans. 5 (1974) 1429–1436, https://doi.org/10.1007/BF02646629.
[30] J.P. Niu, K.N. Yang, X.F. Sun, T. Jin, H.R. Guan, Z.Q. Hu, Denitrogenation during vacuum induction melting refining Ni base superalloy using CaO crucible, Mater. Sci. Technol. 18 (2002) 1041–1044, https://doi.org/10.1179/026708302225004784.
[31] H. Hoshikawa, I. Tanaka, T. Megumi, Refining technology and low temperature properties for high purity aluminum, sumitomo, Kagaku. (2013) 1–12.
[32] R. Harris, W.G. Davenport, Pilot plant scale vacuum distillation of liquid steel to remove copper, Can. Metall. Q. 18 (1979) 303–311, https://doi.org/10.1179/cmq.1979.18.3.303.
[33] E. Ozberk, R.I.L. Guthrie, A kinetic model for the vacuum refining of inductively stirred copper melts, Metall. Trans. B. 17 (1986) 87–103, https://doi.org/10.1007/BF02670822.
[34] C. Edtameir, P. Švec, The role of reactions between crucible and melt during refining of platinum by vacuum induction melting, Can. Metall. Q. 43 (2004) 371–380, https://doi.org/10.1179/cmq.2004.43.3.371.
[35] M. Miyake, T. Hiramatsu, M. Maeda, Removal of phosphorus and antimony in silicon by electron beam melting at low vacuum, Jpn. Inst. Met. 70 (2006) 43–46.
[36] K. Hanazawa, N. Yuge, S. Hiwasa, Y. Kato, Evaporation of phosphorus in molten silicon with electron beam irradiation method, Mater. Trans. 45 (2004) 844–849.
[37] D. Jiang, Y. Tan, S. Shi, W. Dong, Z. Gu, X. Guo, Evaporated metal aluminium and calcium removal from directionally solidified silicon for solar cell by electron beam candle melting, Vacuum 86 (2012) 1417–1422, https://doi.org/10.1016/j.vacuum.2012.01.004.
[38] D. Jiang, S. Shi, Y. Tan, H.M. Noor Ul Huda Khan Asghar, S. Qin, Segregation and evaporation behaviors of aluminum and calcium in silicon during solidification process induced by electron beam, Semicond. Sci. Technol. 30 (2015), https://doi.org/10.1088/0268-1242/30/3/035013.
[39] Y. Tan, X. Guo, S. Shi, W. Dong, D. Jiang, Study on the removal process of phosphorus from silicon by electron beam melting, Vacuum 93 (2013) 65–70, https://doi.org/10.1016/j.vacuum.2012.12.010.
[40] K. Wei, D. Zheng, W. Ma, B. Yang, Y. Dai, Study on Al removal from MG-Si by vacuum refining, Silicon 7 (2015) 269–274, https://doi.org/10.1007/s12633-014-9228-9.
[41] J. Safarian, T.A. Engh, Vacuum evaporation of pure metals, Metall. Mater. Trans. A. 44 (2013) 747–753, https://doi.org/10.1007/s11661-012-1464-2.
[42] C. Zhang, K. Wei, D. Zheng, W. Ma, Y. Dai, Phosphorus removal from upgraded metallurgical-grade silicon by vacuum directional solidification, Vacuum 146 (2017) 159–163, https://doi.org/10.1016/j.vacuum.2017.08.037.
[43] J. Safarian, M. Tangstad, Kinetics and mechanism of phosphorus removal from silicon in vacuum induction refining, High Temp. Mater. Process. 31 (2012) 73–81, https://doi.org/10.1515/htmp.2011.143.
[44] N. Yuge, H. Baba, Y. Sakaguchi, K. Nishikawa, H. Terashima, F. Aratani, Purification of metallurgical silicon up to solar grade, Sol. Energy Mater. Sol. Cells. 34 (1994) 243–250, https://doi.org/10.1016/0927-0248(94)90046-9.
[45] S.S. Zheng, T. Abel Engh, M. Tangstad, X.T. Luo, Separation of Phosphorus from silicon by induction vacuum refining, Sep. Purif. Technol. 82 (2011) 128–137, https://doi.org/10.1016/j.seppur.2011.09.001.
[46] S.S. Zheng, W.H. Chen, J. Cai, J.T. Li, C. Chen, X.T. Luo, Mass transfer of phosphorus in silicon melts under vacuum induction refining, Metall. Mater. Trans. B Process Metall. Mater. Process. Sci. 41 (2010) 1268–1273, https://doi.org/10.1007/s11663-010-9422-0.
[47] S. Zheng, J. Safarian, S. Seok, S. Kim, T. Merete, X. Luo, Elimination of phosphorus vaporizing from molten silicon at finite reduced pressure, Trans. Nonferr. Met. Soc. China. 21 (2011) 697–702, https://doi.org/10.1016/S1003-6326(11)60768-1.
[48] S.-M. Liang, R. Schmid-Fetzer, Modeling of thermodynamic properties and phase equilibria of the Si-P system, J. Phase Equilibria Diffus. 35 (2014) 24–35, https://doi.org/10.1007/s11669-013-0269-3.
[49] E. Photovoltaic, S. Energy, Vacuum removal of the impurities from different silicon melts, in: 26th Eur. Photovolt. Sol. Energy Conf. Exhib. Vac., 2011: pp. 1810–1813. doi:10.4229/26thEUPVSEC2011-2BV.4.3.
[50] A. Hoseinpur, J. Safarian, Phosphorus removal from Al-doped silicon by vacuum refining, in: 35th Eur. Photovolt. Sol. Energy Conf. Exhib. Phosphorus, Bruxel, 2018: pp. 469–472. doi:10.4229/35thEUPVSEC20182018.
[51] X. Peng, W. Dong, Y. Tan, D. Jiang, Removal of aluminum from metallurgical grade silicon using electron beam melting, Vacuum 86 (2011) 471–475, https://doi.org/10.1016/j.vacuum.2011.09.018.
[52] A. Hoseinpur, J. Safarian, Mechanisms of graphite crucible degradation in contact with Si–Al melts at high temperatures and vacuum conditions, Vacuum 171 (2019) 108993, , https://doi.org/10.1016/j.vacuum.2019.108993.
[53] T. Miki, K. Morita, N. Sano, Thermodynamics of phosphorus in molten silicon, Metall. Mater. Trans. B. 27 (1996) 937–941.
[54] A.I. Zaitsev, A.D. Litvina, N.E. Shelkova, Thermodynamic properties of Si-P melts, High Temp. 39 (2001) 227–232, https://doi.org/10.1023/A:1017570715796.
[55] M.E. Schlesinger, The thermodynamic properties of phosphorus and solid binary phosphides, Chem. Rev. 102 (2002) 4267–4301, https://doi.org/10.1021/cr000039m.
[56] S.K. Upadhyay, Chemica kinetics and reactions dynamics, 2006.
[57] O. Knacke, I.N. Stranski, The mechanism of evaporation, Prog. Met. Phys. 6 (1956) 181–235, https://doi.org/10.1016/0502-8205(56)90007-7.
[58] R. Harris, Numerical simulation of vacuum refining of liquid metal, Can. Metall. Q. 27 (2013) 169–178, https://doi.org/10.1179/cmq.1988.27.3.169.
[59] P. Rahimi, Kinetics of evaporation: statistical rate theory approach, Int. J. Thermodyn. J. Thermodyn. 8 (2005) 1–4.
[60] A.H. Persad, C.A. Ward, Expressions for the evaporation and condensation coefficients in the Hertz-Knudsen relation, Chem. Rev. 116 (2016) 7727–7767, https://

doi.org/10.1021/acs.chemrev.5b00511.
[61] M. Olette, Vacuum distilation of minor elements from liquids ferrous alloys, in: G.R. StPierre (Ed.), Phys. Chem. Process Metall., Interscience, NewYorks, 1961, pp. 1065–1087.
[62] S. Shi, W. Dong, X. Peng, D. Jiang, Y. Tan, Evaporation and removal mechanism of phosphorus from the surface of silicon melt during electron beam melting, Appl. Surf. Sci. 266 (2013) 344–349, https://doi.org/10.1016/j.apsusc.2012.12.022.
[63] Q. Wang, W. Dong, Y. Tan, D. Jiang, C. Zhang, X. Peng, Impurities evaporation from metallurgical-grade silicon in electron beam melting process, Rare Met. 30 (2011) 274–277, https://doi.org/10.1007/s12598-011-0382-6.
[64] E. Ozberk, R.I.L. Guthrie, Application of vacuum refining in copper production, Mater. Sci. Technol. 1 (1985) 12–18, https://doi.org/10.1179/mst.1985.1.1.12.
[65] S. Favre, I. Nuta, G. Chichignoud, K. Zaïdat, C. Chatillon, Removing phosphorus from molten silicon: a thermodynamic evaluation of distillation, ECS J. Solid State Sci. Technol. 5 (2016) P129–P137, https://doi.org/10.1149/2.0361602jss.